Title: Detection of Eye Blink Artifacts from Single Prefrontal Channel Electroencephalogram

Author: Won-Du Chang Ho-Seung Cha Kiwoong Kim Chang-Hwan Im

PII: S0169-2607(15)00271-0
DOI: http://dx.doi.org/doi:10.1016/j.cmpb.2015.10.011
Reference: COMM 4001

To appear in: *Computer Methods and Programs in Biomedicine*

Received date: 26-6-2015
Revised date: 24-9-2015
Accepted date: 14-10-2015

Please cite this article as: W.-D. Chang, H.-S. Cha, K. Kim, C.-H. Im, Detection of Eye Blink Artifacts from Single Prefrontal Channel Electroencephalogram, *Computer Methods and Programs in Biomedicine* (2015), http://dx.doi.org/10.1016/j.cmpb.2015.10.011

Research highlights

A novel method to detect eye blink artifacts from a single-channel frontal EEG signal was proposed.

Overall accuracy of detecting epochs contaminated by eye blink artifacts was markedly increased.

An online experiment showed that our method is useful for headband-type wearable EEG applications.

A MATLAB package of our library and sample data is open for free download.

Detection of Eye Blink Artifacts from Single Prefrontal Channel Electroencephalogram

Won-Du Chang[1], Ho-Seung Cha[1], Kiwoong Kim[2], Chang-Hwan Im[1] *

[1] Department of Biomedical Engineering, Hanyang University, Seoul, Republic of Korea

[2] Korea Research Institute of Standard and Science (KRISS), Daejeon, Republic of Korea

*Corresponding author:

Chang-Hwan Im, Ph.D.

Department of Biomedical Engineering, Hanyang University

222 Wangsimni-ro, Seongdong-gu, Seoul 133-791, Korea

Tel.:+82 2 2220 2322; Fax: +82 2 2296 5943

E-mail address: ich@hanyang.ac.kr (C.H. Im)

Abstract:

Eye blinks are one of the most influential artifact sources in electroencephalogram (EEG) recorded from frontal channels, and thereby detecting and rejecting eye blink artifacts is regarded as an essential procedure for improving the quality of EEG data. In this paper, a novel method to detect eye blink artifacts from a single-channel frontal EEG signal was proposed by combining digital filters with a rule-based decision system, and its performance was validated using an EEG dataset recorded from 24 healthy participants. The proposed method has two main advantages over the conventional methods. First, it uses single-channel EEG data without the need for electrooculogram references. Therefore, this method could be particularly useful in brain-computer interface applications using headband-type wearable EEG devices with a few frontal EEG channels. Second, this method could estimate the ranges of eye blink artifacts accurately. Our experimental results demonstrated that the artifact range estimated using our method was more accurate than that from the conventional methods, and thus, the overall accuracy of detecting epochs contaminated by eye blink artifacts was markedly increased as compared to conventional methods. The MATLAB package of our library source codes and sample data, named Eyeblink Master, is open for free download.

Keywords: electroencephalogram (EEG); electrooculogram (EOG); artifact detection; eye blink

1 Introduction

Eye blinks are one of the most influential sources of artifacts contaminating electroencephalogram (EEG) signals [1–3]. It has been known that eye blinks can easily distort EEG signals, leading to inaccurate topographical maps [4]. Because of the high influence of eye blink artifacts on frontal channel EEG signals, removing eye blink artifacts is regarded as a common and essential preprocessing procedure in EEG studies [3,5,6]. Although theta band is distorted most severely when an EEG signal is contaminated by eye blink artifacts, eye blink artifacts have also been reported to significantly affect alpha and beta band EEG signals [3].

The easiest way to detect eye blink artifacts is simply using a predetermined amplitude threshold [7]. This method classifies an EEG epoch as being artifact contaminated if a portion of the EEG or electrooculogram (EOG) signals in this epoch exceeds an amplitude (or power) threshold. This method is generally applicable to raw, time-domain EEG signals, but it can also be applied to frequency-domain signals [8]. The high simplicity of this method is obviously one of its main advantages. This method is particularly useful when high accuracy is not necessarily required [9], or when source EEG data are abundant and thus rejecting a number of contaminated epochs does not cause any critical problems with the main EEG analysis [10]. One of the major limitations of this method is the low accuracy of "epoch-based" artifact rejection, especially when the peak of the eye blink artifact is not included within an epoch [10]. That is to say, when only part of the eye blink artifact is included in an epoch under consideration, it is generally difficult to accurately determine whether the epoch actually includes a portion of an eye blink artifact, because the artifact contamination cannot be detected when the maximum amplitude of the artifact in an epoch is lower than the threshold value. Moreover, this method has difficulty extracting the range of the eye blink artifacts due to variances in eye blink duration [11]. There have been other methods proposed to

detect epochs contaminated by eye blink artifacts, such as probability distribution and kurtosis [12], correlation between EEG signals of selected channels [13], and artificial neural networks [14]. However, since these methods also determine whether an epoch includes eye blink artifacts (referred to as epoch-unit-based detection in this paper), they have the same limitations as the amplitude thresholding method, such as difficulty in detecting eye blink artifacts when only part of the artifact is included in a given epoch.

Removing artifacts without dividing signals into epochs by utilizing blind source separation methods [1] such as independent component analysis (ICA) [6,8,15] is an alternative approach that can circumvent the limitations of the conventional artifact detection methods described above. The artifacts could be removed from the contaminated EEG signals successfully by excluding the artifact components before re-mixing the decomposed signal [1,16,17]. However, ICA generally requires EEG signals recorded from many channels because of its intrinsic characteristics [18], which make it extremely difficult to remove independent components including artifacts accurately when only a few EEG signals are available.

Recording EEG data from many channels may not be an important issue in a laboratory or clinical environment, where there are high-end EEG recording devices with a large number of channels and well-motivated participants who have agreed to participate in experiments with long durations. Recently, however, the advancement of modern sensors and wireless technology is expediting the development of novel applications of EEG that do not necessarily require a laboratory setting, such as measuring the brain activity of healthy persons during daily life, at work or during specific cognitive/emotional tasks [19–22]. Since these EEG applications commonly require wireless EEG recording devices that are easy to wear and comfortable for long-term use, headband-type or headset-type EEG devices with a few electrodes covering only the prefrontal area of the brain has been often preferred in many studies [23–28]. It is also noteworthy that simple system setup is becoming an

important issue in recent brain-computer interface studies [29,30]. These types of portable EEG recording devices are not only inherently prone to eye blink artifacts, but also generally do not have an EOG channel that can be employed as a useful artifact indicator; thus, the accurate detection and rejection of eye blink artifacts is of great importance.

In the present study, we propose a novel method to detect eye-blink-related waves precisely from a single frontal-channel EEG signal, which can potentially be applied to a variety of daily-life EEG applications. The proposed method was based on the combination of digital filters and a rule-based decision system. The digital filters were adopted to emphasize waves with specific wave-widths, and the rule-based decision system was developed to recognize eye blinks and to determine the ranges of the blinks. The proposed method is unique in two aspects: first, it uses a single EEG channel without EOG reference, and second, it can accurately estimate the extent of artifact ranges in continuous (online) EEG data. In the following sections, we describe the mathematical details of the proposed method and our procedure for validating it using an EEG dataset acquired from 24 healthy participants while they were performing a specific cognitive task.

2 Materials and Methods

2.1 Summation of Derivatives within a Window (SDW)

An eye blink artifact is formed with a gradual increase and decrease generally within 100 and 500 ms [11,31–33], whereas the EEG signals cover wider frequency ranges (0.5 to 50 Hz and above) [34,35] (see the first figure in Figure 1 for a schematic representation of a contaminated EEG signal).

When a sliding window is set to be large enough to cover multiple ripples of an EEG waveform, as shown in Figure 1, the summation of the first-order derivatives of the raw signal within the sliding window will filter out the ripples. When the sliding window size is set to be approximately half the width of the target eye blink wave and the window slides along the time axis, the filter output (the summation of the first-order derivatives within a sliding window) can distinctly extract the presence of the target wave while suppressing other ripples with smaller periods than the target wave, as depicted in Figure 1.

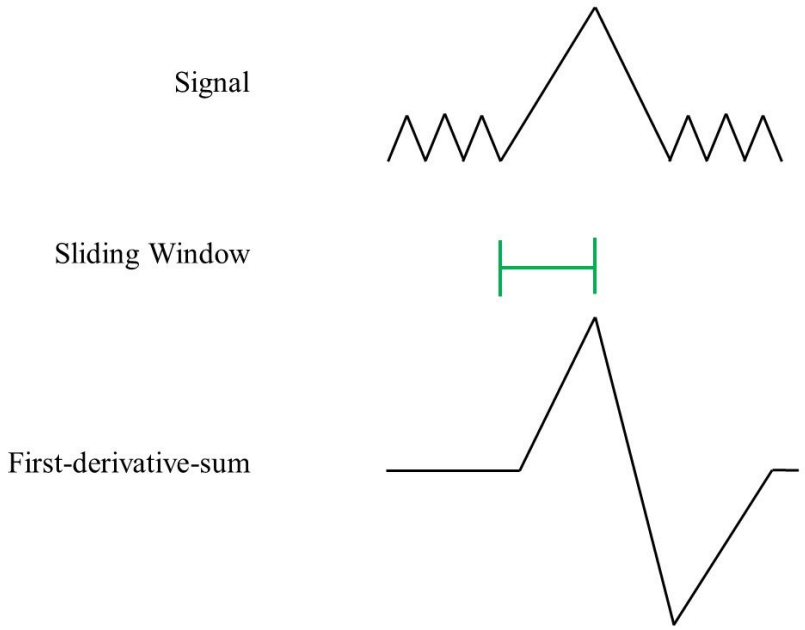

Figure 1. A schematic illustration of the summation of the first order derivative within a window (SDW). When the sliding window size is set to be approximately half the width of the target wave and the window slides along the time axis, the filter output can distinctly extract the presence of the target wave, as depicted here.

A function $F(t)$ representing the "first derivative sum" at a time t can be written as

$$F(t) = \sum_{k=t-n+1}^{t} S(k) - S(k-1), \quad (1)$$

where n is the width of the sliding window and $S(k)$ is the k^{th} sample of the original signal. From now on, let us call this function SDW, denoting the summation of first derivatives within a window. The equation of SDW can be regarded as a kind of the two-point central difference algorithm [36], which was developed to calculate first order derivative in a digital signal.

2.2 Eye Blink Artifact Detection Using SDW

As shown in Figure 1, SDW has maximum and minimum values at the peak point and the last point of the eye blink artifact, respectively, when the size of sliding window is assumed to be half of the artifact width. Therefore, the presence of an eye blink artifact can be determined by comparing the difference between a local minimum and the local maximum that directly precedes it with a predetermined threshold. When Min_i is the i^{th} local minimum value of an SDW time series and Max_i is the local maximum value preceding Min_i, the time range of the artifact, R, can be estimated by

$$R = \{[T(Max_i) - |W|, \quad T(Min_i)] \mid Max_i - Min_i > \theta\}, \quad (2)$$

where $|W|$ is the size of the sliding window, θ is a predetermined threshold, and $T(Max_i)$ and $T(Min_i)$ are the time points of the i^{th} local maximum and minimum, respectively.

2.3 Artifact Determination using Multiple Windows: Multi-window SDW (MSDW)

Theoretically, the ranges of the artifacts can be estimated perfectly if the size of the sliding window is set to exactly half the target-wave range and the shape of the artifacts is assumed to be a triangular pulse shape, as shown in Figure 1. In practice, however, there is wide variation in the ranges of the artifacts even in data from the same participant. Moreover, the artifacts often have irregular forms different from that shown in Figure 1, which causes severe variation in the results of SDW. Figure 2 shows the influence of the sliding window size on the resultant SDW when a variety of artifacts with various sizes and shapes are assumed to be included in the source EEG data. The data used for this simulation were generated by adding artificial artifacts to a background ripple signal with a relatively higher frequency and smaller amplitude than those of the artifacts. The first five artificial artifacts had a regular shape (triangular pulse shape), but had different widths ranging from 62.5 to 312.5 seconds (4, 8, 12, 16, and 20 points with the 64-Hz sampling rate). The last artificial artifact was assumed to include two closely located peaks, because similar shapes are frequently observed in practical EEG data (see Figure 3 for an example).

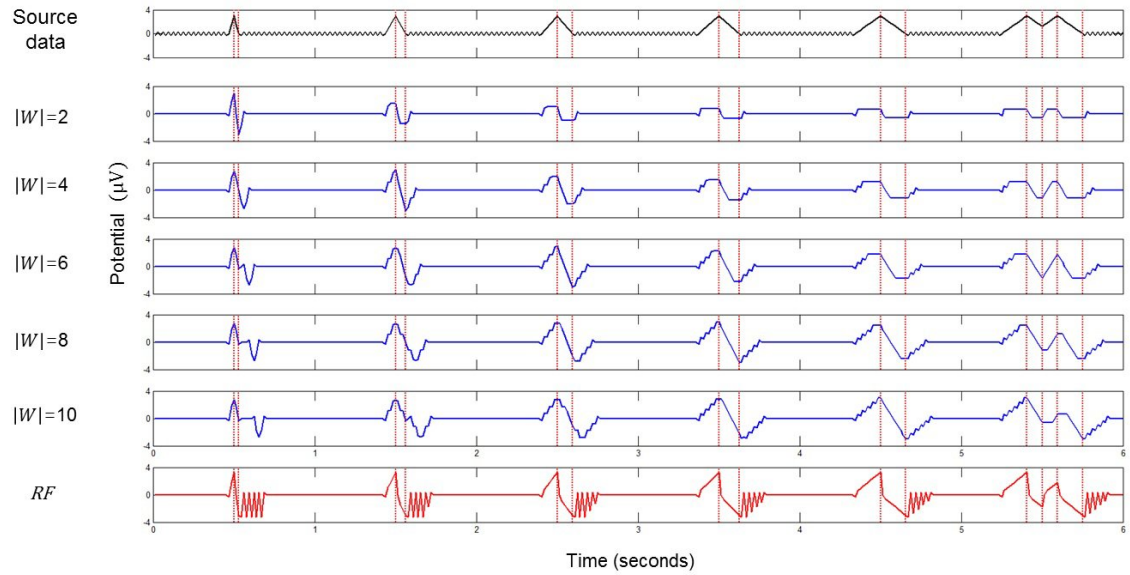

Figure 2. Artificially generated source data (artificial EEG data with artifacts) and SDWs evaluated with different sliding window sizes, $|W|$. The window sizes (2, 4, 6, 8, and 10) represent the number of time samples when a 64-Hz sampling rate was used. The vertical dashed lines are drawn at the time points of wave peaks, valleys, and endpoints.

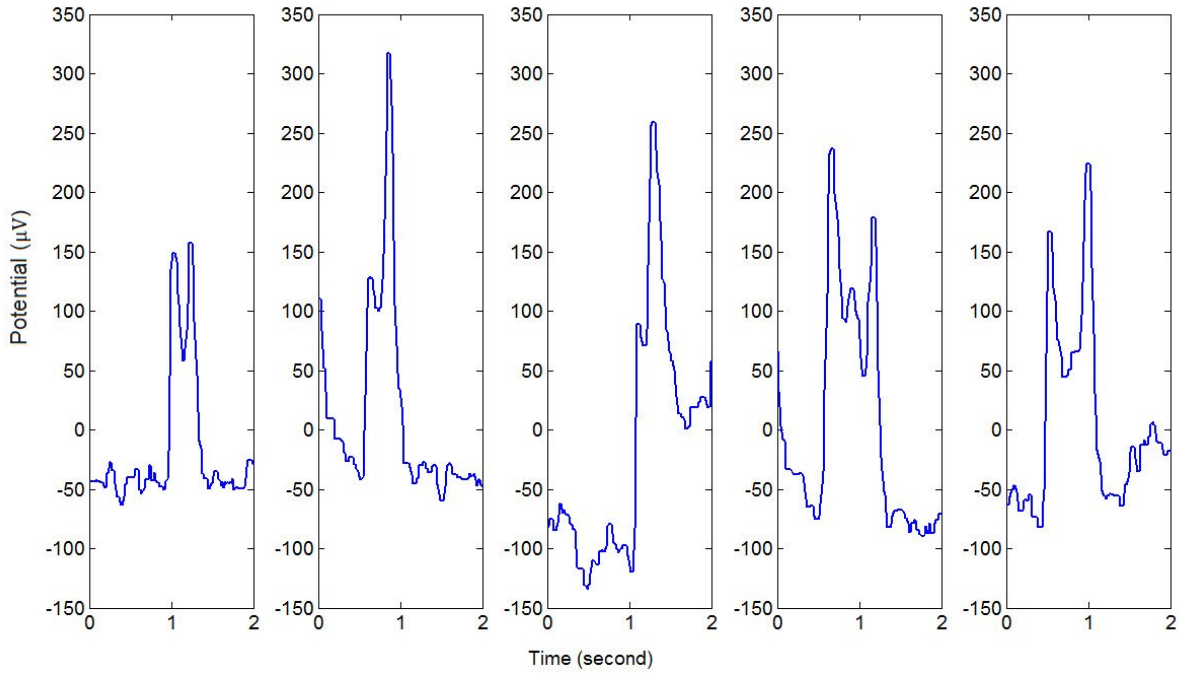

Figure 3. Examples of eye blink artifacts included in real EEG signals having multiple peaks

In this preliminary test, the ideal SDW waveforms (as shown in Figure 1) were observed only when the window size $|W|$ was set to be the same as the half-width of the artifact and the shape of the artifact was assumed to be a single triangular pulse. From the simulation results, it could be readily observed that the local maximum in the SDW waveform is maximized when the window size becomes the same as the half-width of the artifact. Based on this finding, we developed an empirical procedure to determine the optimal window size for calculating SDW at time t. The detailed steps are given below:

1. For each time point, calculate SDWs with different sliding window sizes ranging from m to M, where m and M are the minimum and maximum lengths, respectively, of the window sizes to be tested. Let $F_{|W|}$ denote an SDW with a window size of $|W|$.
2. Choose the $F_{|W|}$ having the maximum value at time t and satisfying the following conditions, and denote it as $RF(t)$:
    a. The numbers of local minimum and maximum within the range, t and $t - |W|$, should be the same.
    b. All the first derivatives between times t and $t - |W| + 1$ should be placed within a range between $S'(t - |W| + 1)$ and $S'(t)$, where $S'(t)$ represents the first derivative

of the original signal at time t.

3. If the above conditions are not met, $F_{|m|}$ is chosen.

4. If the maximum value of $F_{|W|}$ is obtained at multiple values of $|W|$, the smallest $|W|$ is selected.

The above process is repeatedly applied for every t, and the selected window size at a time t is denoted by $|W_{RF(t)}|$.

For the artifacts with irregular forms, the resultant SDW waveforms show multiple local maxima and local minima for a single artifact, as shown in Figure 2. Therefore, there can be multiple maxima before the *i*-th local minimum point. To consider this, the time range of the artifact was redefined as

$$R = \left\{ \left[T(Max_{i-j}) - \left| W_{RF\left(T(Max_{i-j})\right)} \right|, \; T(Min_i) \right] \;\middle|\; Max_{i-j} - Min_i > \theta \right\}, \quad (3)$$

where j is an integer that maximizes $Max_{i-j} - Min_i$ subject to $j \geq 0$ and $T(Max_{i-j}) - T(Min_i) \leq M$, where $T(Max_i)$ and $T(Min_i)$ are the time points of the i^{th} local maximum and minimum, respectively. Any j is rejected if the range $\left[T(Max_{i-j}) - \left| W_{RF\left(T(Max_{i-j})\right)} \right|, \; T(Min_i) \right]$ partially overlaps another range. If a range is fully included in another range, the included range is discarded. For more comprehensive understanding of our procedure, please download the library source codes freely downloadable at http://cone.hanyang.ac.kr/BioEST/Eng/EyeblinkMaster.zip.

2.4 Conventional Methods I - Amplitude Thresholding Method

To evaluate the performance of the proposed method quantitatively, the amplitude thresholding method that has been widely used in EEG preprocessing [37–42] was implemented. This method simply classifies a signal epoch as being contaminated if it contains values over a certain threshold. The threshold was used as a variable in the experiments for the comprehensive evaluation of the method. We applied a bandpass filter (Butterworth, first order) with 2- and 10-Hz cutoffs to enhance the accuracy of the amplitude thresholding method. The type, order, and cutoff frequencies of the filter were determined empirically.

2.5 Conventional Methods II - Template Matching Method

The template matching method is a widely used method to detect specific patterns contained in a signal. We used a general implementation of the method [43] for comparison, with different dissimilarity metrics: correlation [44], root-mean-square error (RMSE), and dynamic time warping (DTW) [9].

The process of the template matching method used in this study is given below:

1. At each sampling point, calculate dissimilarity between a predetermined template and a subsequence of EEG signal which starts at the point. The length of the subsequence is set to be the same as that of the template. A sequence of dissimilarity can be obtained as the results.
2. Find all local minima of the dissimilarity sequence. The subsequences around the minima are regarded as candidates of time interval including eye blink artifacts.
3. Classify the candidates as eye blink artifacts if their corresponding minima are smaller than a threshold.

One of the limitations of template matching is that its accuracy is highly dependent on the template selection. Though templates can be selected manually by an expert or generated automatically by an automated system, we selected templates which yielded the best accuracy in our previous study [43]. Please note the best templates were selected individually for each method.

2.6 Data Acquisition and Preprocessing

To verify the proposed method, EEG data acquired from 24 participants (eighteen males and six females) [43], aged between 22 and 31, were used. The data were collected using an ActiveTwo^{TM} system (BioSemi, Netherlands) at a sampling rate of 2048 Hz. During the data collection, the participants performed 'spot-the-difference' tasks, which was to find differences between two horizontally aligned images in 15 seconds. This was repeated ten times with 15 seconds interval for each participants. Data obtained at three channels were used for this study. The channels were Fp1, Fp2, and EOG_v that was placed below right eye. Because we used active electrodes, electrode impedances could not be measured [45]. A common mode sense (CMS) and driven right leg (DRL) electrode loop were served as ground and reference, respectively, where the both CMS and DRL were placed to the closest approximation of a POz electrode (the CMS was placed between POz and PO3, the DRL was placed between POz and PO4).

Before the data acquisition, a comprehensive summary of the experimental procedures and protocols were explained to each participant. All participants signed a consent form and received monetary reimbursement for their participation. The study was approved by the institutional review board (IRB) committee of Hanyang University. A total of 8,099 seconds of data (including data obtained before and after the task) acquired from 24 participants was used to compare the performance of different eye blink artifact detection algorithms. Among two prefrontal channels (Fp1 and Fp2), only Fp2 channel was used in this study because the artifacts observed in both channels

showed very similar shapes (see Fig. 4).

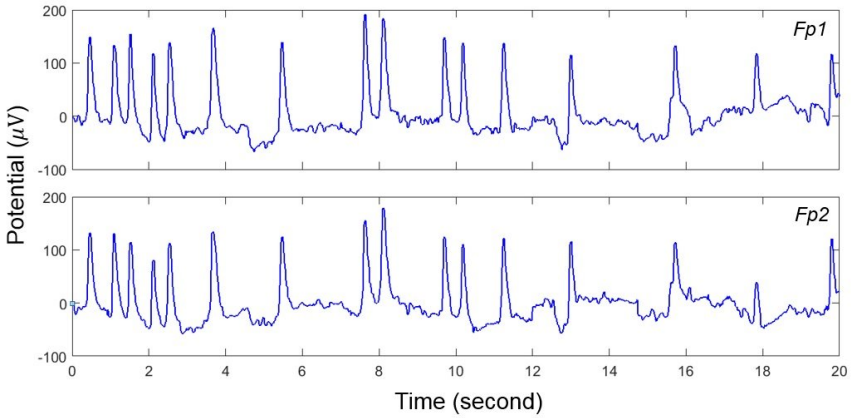

Figure 4. Eye blink artifacts observed in prefrontal channel EEG.

The collected EEG data were high-pass filtered at 0.1 Hz (Butterworth, first order), downsampled into 64 Hz to reduce the amount of data, and median filtered to smooth out tiny waves. We used a width-5 median mask for this purpose, which means the median filter had a width of about 7.81 ms.

A ground truth (or gold standard) dataset had been constructed by two independent researchers before the development of algorithms (the same dataset was already used in [43]). Eye blink regions in this dataset were marked according to the literature [11,31,32,46,47] based on both the Fp2 data and the vertical electrooculogram (EOG_v) signals recorded from an electrode attached below a right eye. The criteria to determine that a wave was an eye blink artifact were as follows:

1. A positive sharp wave over 50 μV during 100 – 500 ms in Fp2,
2. A negative wave peak on EOG_v within the range of the wave in Fp2, and
3. A gradual increase and decrease from the starting point to the top of the peak and from the top to the end point, respectively.

In some cases, it was difficult to determine whether an artifact originated from an eye blink or not; such patterns were classified as ambiguous artifacts (e.g., those with very long durations, and those

with different timings or patterns between Fp2 and EOG_v). Ambiguous artifacts were ignored irrespective of whether a method detected them as an eye blink artifact or not, so that they would not influence the accuracy calculations. The ground truth dataset had been constructed before the proposed method was developed, and thus the dataset was not biased at all.

3 Results

3.1 Detection of Contaminated Epochs

To validate the feasibility of the proposed method, epochs contaminated by eye blink artifacts were detected using the various methods described in Section 2. Test EEG signals acquired from 24 participants were segmented into epochs, each with a one-second duration. To search for the contaminated epochs, the ranges of the artifacts were estimated first, and then epochs including a part of the estimated artifact ranges were detected. Examples of the artifact ranges estimated using the proposed method are shown in Figure 5.

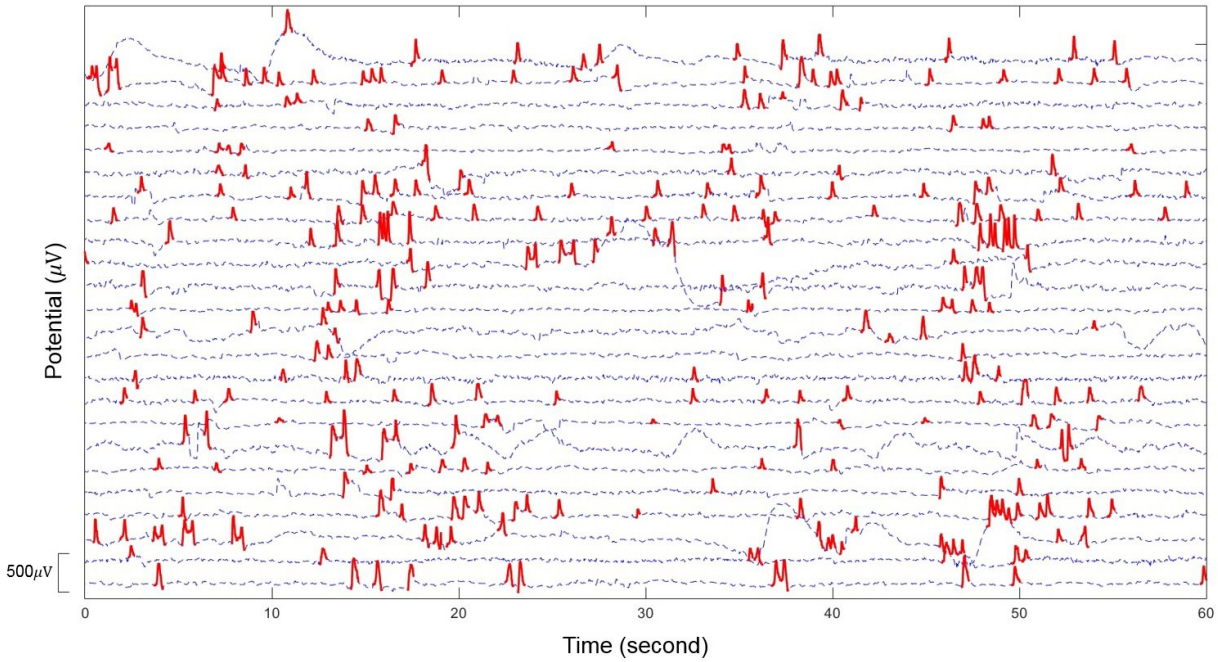

Figure 5. Examples of detected eye blink artifacts. EEG signals of 24 participants recorded at the Fp2 channel are plotted sequentially (the first signal is from participant 1, and the bottom one is from participant 24), and the detected artifact ranges are marked with thick red lines.

The receiver operating characteristic (ROC) curves were evaluated for each individual and then averaged across all participants to generate the average ROC curve of each method, as depicted in Figure 6. The individual ROC curves were calculated by increasing the number of epochs to be detected from 0 to the total number of epochs. The ROC curves were used as the performance measure because the number of contaminated epochs is generally unknown in practical cases. When the number of epochs to be detected is zero, the false positive error rate (FPR) becomes zero, whereas the true positive rate (TPR) becomes one when the number of epochs to be detected equals the total number of epochs. The false positives were counted when uncontaminated epochs were misidentified as contaminated ones, while the false negatives were counted when contaminated epochs were not identified. TPR is calculated by subtracting false negative rates (FNR) from 1. To calculate ROC curve for all the participants, the ROC curves of each participant were calculated and then TPRs were averaged for each FPRs, since the numbers of eye blinks were different for each participant's data.

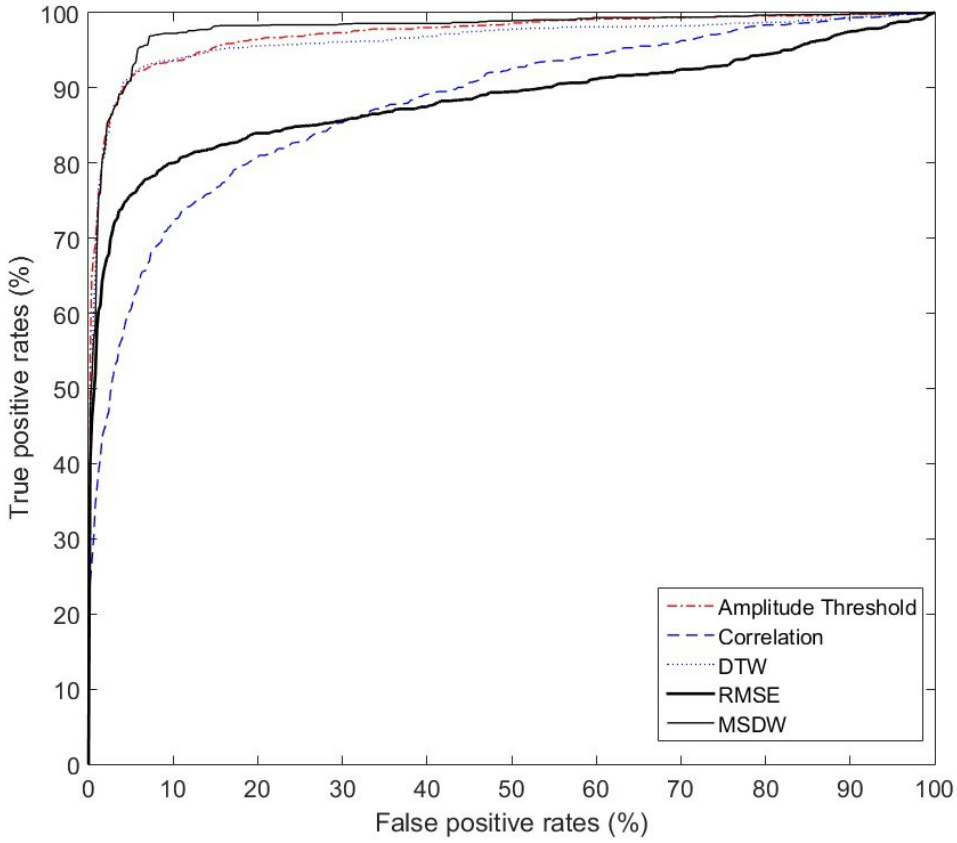

Figure 6. ROC curves of five different methods for the detection of contaminated epochs, where trade-offs between false positive rates and true positive rates are presented. The proposed method is denoted as MSDW (multiple-window SDW).

The calculated ROC curves in Figure 6 show that the proposed MSDW method has a similar trend to the amplitude thresholding method and DTW when FPR is smaller than 5%, but the differences in mean TPR increase afterwards. The proposed method outperformed all other methods with respect to equal error rate (EER) [48], which represents the error value when FPR is equal to FNR. Please note that the EERs were calculated for each individual for this comparison study. It was validated using repeated measures ANOVA that the EER differs among methods ($F_{(1.716,\ 39.467)}$=24.195, p<0.001, Greenhouse-Geisser correction), and the post-hoc paired t-test analysis with Bonferroni correction

revealed that the EER of the proposed method (3.98% ± 2.90%) was significantly smaller than other methods (amplitude thresholding method: 6.76% ± 3.72, p=0.001; DTW: 6.55% ± 3.48, p <0.05; correlation method: 18.93% ± 7.35%, p <0.001; RMSE method: 15.36% ± 13.21%, p <0.01).

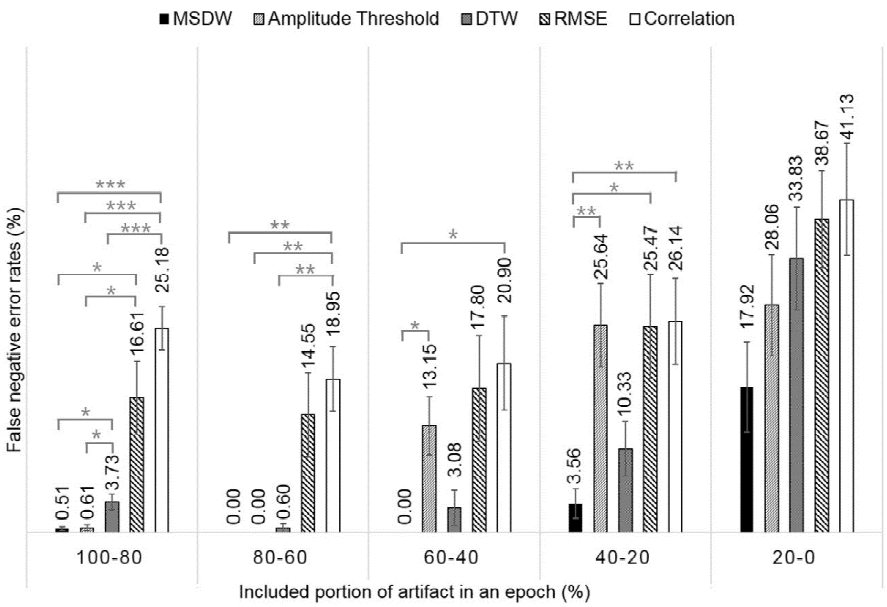

Figure 7. FNR changes with respect to the portion of an artifact included in an epoch. Error bars represent standard errors. * p<0.05, ** p<0.01, *** p<0.001.

To further demonstrate the superiority of the proposed method, we investigated the changes of the detection accuracy with respect to the portion of an artifact included in an epoch. Figure 7 shows the FNR differences with respect to the portion of artifact within an epoch, when FPR is forced to be under 10%. The proposed method kept the mean FNR to be lower than 1% when an artifact contaminated more than 40% of an epoch, whereas the mean FNR of amplitude thresholding method increased dramatically when an artifact is included in less than 60% of an epoch. A two-way ANOVA with repeated measures (methods, artifact portion) showed a significant effect in methods ($F_{(2.362, 51.960)} = 10.233$, $p < 0.001$, Greenhouse-Geisser correction), and post-hoc analysis (Bonferroni

corrected) revealed that the proposed method had significantly lower FNR than amplitude thresholding method ($p < 0.001$), correlation method ($p < 0.001$), and RMSE method ($p = 0.050$). One-way repeated measures ANOVA showed significant effects in methods at each portion group except the range between 0 and 20% (80-100%: $F_{(1.677, 38.579)} = 24.627$, $p < 0.001$; 60-80%: $F_{(1.885, 43.351)} = 10.414$, $p < 0.001$; 40-60%: $F_{(1.885, 43.351)} = 5.271$, $p < 0.01$; 20-40%: $F_{(4, 92)} = 5.567$, $p < 0.001$). The statistical values were corrected with Greenhouse-Geisser method when the assumption of sphericity had been violated. Post-hoc analysis (Bonferroni) revealed that MSDW showed significantly better performance than amplitude thresholding when the portions are between 40 and 60% ($p < 0.05$), and 20 and 40% ($p < 0.01$); whereas it outperformed DTW when the portion is between 80 and 100% ($p = 0.010$), RMSE method when the portions are between 80 and 100% ($p < 0.05$) and 20 and 40% ($p < 0.05$), and correlation method when the portions are between 80 and 100% ($p < 0.001$), 60 and 80% ($p = 0.001$), 40 and 60% ($p < 0.05$), and 20 and 40% ($p < 0.01$).

3.2 Estimation of Artifact Range

Since one of the hypotheses of this study was that our proposed method would estimate the ranges of the artifacts more accurately than the conventional methods, we compared how accurately each method could estimate the ranges of eye blink artifacts. However, it is generally very difficult to define the boundaries of each artifact exactly, because the artifacts are mixed up with original EEG signals when only a single-channel frontal EEG electrode is used for the recording. Therefore, in this study, the estimation accuracy was evaluated by introducing an “error tolerance” concept.

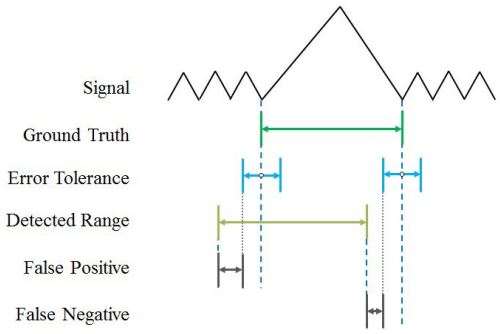

Figure 8. A schematic diagram to illustrate the concepts of error tolerance, false positives, and false negatives. Errors that occurred within the error tolerance ranges were considered as if they were correct.

Figure 8 is a schematic diagram that illustrates the basic concept of error tolerance. In the figure, "ground truth" denotes the exact range of an artifact. When a certain error tolerance is given at the two borders of the artifact, actual errors (false positives or false negatives) found within these two "Error Tolerance" ranges are tolerable, i.e., they are regarded as correctly detected artifact ranges. In this study, the error tolerance ranges within the ground truth range were termed the false negative tolerance (FN tolerance) because false negative errors (FN) are tolerated within these ranges. Likewise, the error tolerance ranges outside the ground truth range were named the false positive tolerance (FP tolerance) because false positive errors (FP) are tolerated within them. Note that the FN tolerance and FP tolerance do not need to be identical. The FN tolerance was represented by the proportion of the FN tolerance to the length of the ground truth of each artifact, because each artifact width was not a fixed value, but a varying one. In contrast, the FP tolerance was represented by a physical time (in seconds) from the borders of the ground truth of each artifact. Figure 8 also shows an example of how FPR and FNR are calculated when a certain error tolerance is given. As shown in the figure, when the FP tolerance is large, the FP of the detected range becomes small. Likewise, when the FN tolerance is large, the FN of the detected range becomes small. FNR can be readily

evaluated by dividing the total number of FN by the total number of the artifacts, and FPR can be evaluated by dividing the total time length of FP by the time length of clean EEG (i.e., outside of the artifact region). As in the previous epoch-based evaluation study, each individual participant's ROC curves were evaluated by increasing the number of artifacts to be detected, and then the curves were averaged across all participants to obtain the grand-averaged ROC curve of each method.

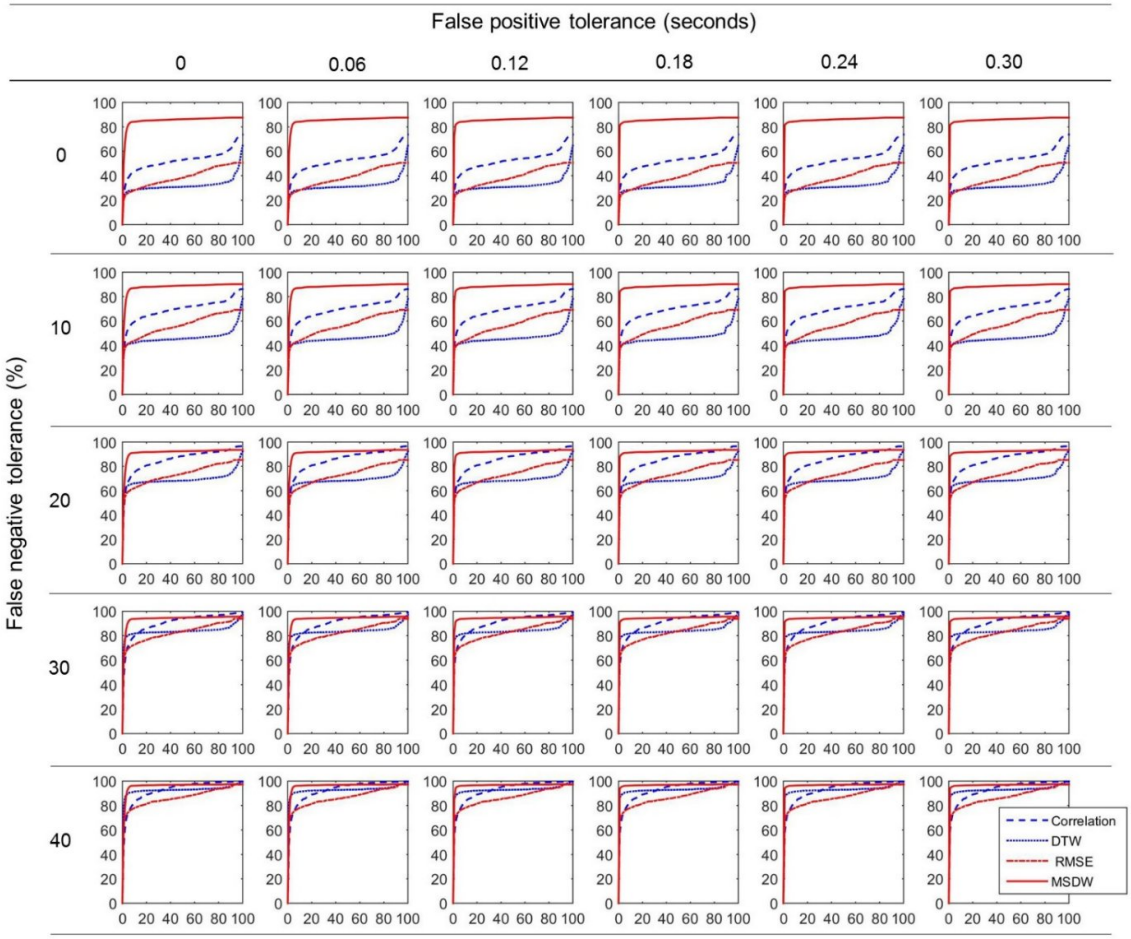

Figure 9. ROC curves with respect to different pairs of false positive tolerances and false negative tolerances in the estimation of the artifact ranges. The abscissa of each curve represents the false positive error rate (FPR, as a percentage), and the ordinate represents the true positive rate (TPR, as a percentage).

Table 1. Areas under curve with respect to different pairs of false positive and false negative tolerances in the estimation of the artifact ranges.

			False positive tolerance (seconds)					
			0	0.06	0.12	0.18	0.24	0.3
False negative tolerance (%)	0	Correlation	52.48±20.32	52.63±20.36	52.82±20.42	52.93±20.41	53.09±20.38	53.25±20.43
		DTW	32.10±23.95	32.19±23.96	32.33±23.95	32.57±23.82	32.82±23.74	32.85±23.77
		RMSE	38.81±18.55	38.91±18.60	39.01±18.63	39.11±18.61	39.20±18.66	39.27±18.69
		MSDW	85.01±10.34	85.28±10.38	85.61±10.47	85.74±10.51	85.75±10.51	85.75±10.51
	10	Correlation	69.39±17.02	69.56±17.06	69.76±17.15	69.87±17.15	69.99±17.10	70.10±17.15
		DTW	46.51±24.83	46.61±24.83	46.75±24.80	46.98±24.64	47.20±24.58	47.23±24.61
		RMSE	56.61±20.41	56.71±20.43	56.83±20.45	56.95±20.39	57.04±20.42	57.10±20.45
		MSDW	87.70±8.89	87.96±8.92	88.30±8.99	88.43±9.03	88.44±9.03	88.44±9.03
	20	Correlation	85.46±11.29	85.63±11.32	85.83±11.40	85.91±11.39	85.99±11.37	86.07±11.39
		DTW	69.18±24.22	69.27±24.22	69.39±24.16	69.56±23.93	69.68±23.88	69.70±23.89
		RMSE	73.34±20.70	73.43±20.71	73.55±20.69	73.66±20.61	73.73±20.61	73.79±20.62
		MSDW	91.17±7.26	91.44±7.28	91.78±7.33	91.90±7.37	91.92±7.37	91.92±7.37
	30	Correlation	90.38±5.40	90.55±5.45	90.74±5.55	90.81±5.56	90.88±5.55	90.95±5.55
		DTW	83.69±17.82	83.78±17.81	83.87±17.73	83.99±17.53	84.07±17.48	84.08±17.48
		RMSE	82.58±18.76	82.68±18.75	82.79±18.70	82.89±18.59	82.96±18.59	83.01±18.57
		MSDW	93.55±4.63	93.81±4.64	94.15±4.69	94.27±4.71	94.28±4.71	94.28±4.71
	40	Correlation	92.60±4.00	92.76±4.04	92.96±4.11	93.02±4.12	93.08±4.09	93.15±4.07
		DTW	92.61±8.92	92.69±8.91	92.77±8.85	92.85±8.74	92.89±8.71	92.89±8.71
		RMSE	86.42±17.59	86.52±17.57	86.62±17.51	86.71±17.39	86.77±17.38	86.82±17.36
		MSDW	95.67±2.94	95.94±2.91	96.28±2.90	96.39±2.93	96.40±2.93	96.40±2.93

Figure 9 and Table 1 show the ROC curves and the corresponding area under curves (AUCs) of each method when different combinations of FP and FN tolerances were assumed. As expected, the AUCs became smaller when either FN tolerance or FP tolerance increased. The effect of FN tolerance on the ROC curves was obviously larger than that of FP tolerance. This is because FP does not necessarily occur around the borders of the actual artifacts. Most importantly, the proposed method outperformed all of the other methods regardless of the error tolerances. A three-way ANOVA with repeated measures (methods, FN tolerance, and FP tolerance) showed a significant effect in methods ($F_{(2.553,\ 58.719)} = 19.631$, $p < 0.001$, Greenhouse-Geisser correction), and post-hoc analysis (Bonferroni) revealed that the proposed method had significantly larger AUC than all other methods at $p < 0.001$ (regardless of the error tolerances).

4 Discussion

In this study, we proposed a novel method to detect eye blink artifacts and estimate their widths, and investigated its feasibility in comparison with conventional methods such as amplitude thresholding and template matching methods based on root-mean-square error (RMSE), correlation, and dynamic time warping (DTW). Two experimental studies to detect contaminated epochs and estimate artifact ranges in an EEG dataset acquired from 24 healthy participants were conducted using various methods, and the results were compared using receiver operating characteristic (ROC) curves. Our experimental results showed that the ranges of eye blink artifacts could be estimated more accurately with our proposed method than with any of the conventional methods used for comparison, and therefore, the overall accuracy of detecting epochs contaminated by eye blink artifacts was markedly higher with the proposed method as compared to those for the conventional methods.

Our study has four main contributions. First, it demonstrated the precise and robust detection of eye blink artifacts from a single-channel frontal EEG signal without the need for EOG data. Most recent studies, including those using independent component analysis (ICA), have employed multi-channel EEGs to detect or remove eye blink artifacts from EEG data. However, considering that large numbers of EEG channels may not always be available in practical EEG applications, our proposed algorithm could be a useful tool to enhance the overall quality and reliability of modern wearable EEG devices and applications. Our proposed algorithm cannot remove eye blink artifacts, but can detect and reject epochs or time ranges contaminated by eye blink artifacts in some practical wearable EEG applications in which the rejection of contaminated EEG epochs or time ranges is does not affect the overall performance and the error tolerance is acceptable to the experimenters.

Second, the traditional belief that the amplitude thresholding method is sufficient for detecting

epochs contaminated by eye blink artifacts [9] was brought into question once again, following the report of [10]. It was also shown that the error rates increased rapidly as the distance between the artifact peak and the epoch borders increased when detecting contaminated epochs [10]. In the current study, the proposed algorithm outperformed the conventional amplitude thresholding method in the accuracy of detecting artifact-contaminated epochs. As aforementioned, the amplitude thresholding method cannot accurately determine whether an epoch includes an eye blink artifact when only part of the eye blink artifact is included in the epoch and the maximum amplitude of the artifact in the epoch is lower than the threshold value. Contrary to the amplitude thresholding method, the proposed method can detect epochs contaminated by eye blink artifacts with higher accuracy since it estimates the ranges of eye blink artifacts accurately.

Third, the artifact ranges in continuous EEG data could be estimated without using any templates. In contrast to the template matching methods, which require additional procedures for template selection, the proposed method does not require any complicated procedures except for the determination of an individual threshold value. Moreover, the proposed method outperformed any of the evaluated template matching methods with their best selected templates in detecting the ranges of eye blink artifacts.

Fourth, a novel approach to detect eye blink artifacts is proposed, which has the potential to be extended into a variety of practical EEG applications. The proposed algorithm simply uses a rule-based approach with a combination of digital filters. Because the proposed algorithm does not require any complex mathematical calculations such as principal component analysis or ICA, the whole procedure can be implemented with low complexity. Therefore, it is expected that the proposed algorithm can be readily applied to various online (real-time) applications. The proposed algorithm was implemented under MATLAB^{TM} (The Mathworks, Inc.) environment, and the implemented MATLAB library files with a comprehensive manual and sample data are freely

available for download at http://cone.hanyang.ac.kr/BioEST/Eng/EyeblinkMaster.zip. We invite researchers who are interested in our study to download and use our library.

Moreover, in order to further demonstrate the applicability of the proposed method to practical real-time applications, we implemented online eyeblink detection software compatible with a wireless EEG device (EnoBio, Neuroelectrics, Spain). The demonstration movie file is attached to this manuscript as a supplementary movie file or can be downloaded at http://cone.hanyang.ac.kr/BioEST/Eng/Eyeblinkmaster.mpg.

There are some related topics that we would like to investigate in the future studies. First, fuzzy classification would be helpful if users wish to apply different approaches for removing ambiguous artifacts. Second, there are a group of algorithms named single-channel ICA to separate independent sources from a single-channel signal [49–51]. The first single channel ICA algorithm [49] was developed under the premise that the sources are stationary and disjoint in the frequency domain [50], whereas recent algorithms utilize signals decomposed using wavelet transform or empirical mode decomposition as if they are observed signals [50,51]. Although these algorithms are data dependent and thus should be verified with a large number of data, a promising result [51] for electrocardiograph artifact removal from electromyogram showed the possibility that these algorithms can be potentially utilized for eye blink artifact removal in the near future. Lastly, an automatic thresholding algorithm must be developed for the proposed method to be fully automatic. Since the proposed method does not include a thresholding algorithm, it requires an empirically determined threshold value (denoted by θ in this study) for each individual dataset to utilize it for a practical use (e.g. determining the threshold value from the few first artifacts in the given data). In our future studies, several algorithms to determine the best threshold values (e.g., Kim and McNames 2007) will be tested or a new algorithm for the automatic threshold determination will be developed. We also plan to apply our proposed method to practical mobile EEG applications in the near future.

Acknowledgements

This work was supported in part by the ICT R&D program of MISP/IITP [10045452, Development of Multimodal Brain-Machine Interface System Based on User Intent Recognition] and in part by the KRISS-WCL project (Development of Measurement Technology for Cognitive Process). The authors would like to thank Dr. Do-Won Kim for his advice on statistical analysis.

References

[1] S. Hoffmann, M. Falkenstein, The correction of eye blink artefacts in the EEG: a comparison of two prominent methods, PLoS One. 3 (2008) e3004.

[2] J.W. Bang, J.-S. Choi, K.R. Park, Noise reduction in brainwaves by using both EEG signals and frontal viewing camera images, Sensors. 13 (2013) 6272–6294.

[3] D. Hagemann, E. Naumann, The effects of ocular artifacts on (lateralized) broadband power in the EEG, Clin. Neurophysiol. 112 (2001) 215–231.

[4] K.L. Coburn, M. a. Moreno, Facts and artifacts in brain electrical activity mapping, Brain Topogr. 1 (1988) 37–45. doi:10.1007/BF01129338.

[5] A. Mognon, J. Jovicich, L. Bruzzone, M. Buiatti, ADJUST: An automatic EEG artifact detector based on the joint use of spatial and temporal features, Psychophysiol. 48 (2010) 229–240.

[6] T.-P. Jung, S. Makeig, M. Westerfield, J. Townsend, E. Courchesne, T.J. Sejnowski, Removal of eye activity artifacts from visual event-related potentials in normal and clinical subjects, Clin. Neurophysiol. 111 (2000) 1745–1758.

[7] H. Nolan, R. Whelan, R.B. Reilly, FASTER: Fully automated statistical thresholding for EEG artifact rejection, J. Neurosci. Methods. 192 (2010) 152–162.

[8] A. Delorme, T. Sejnowski, S. Makeig, Enhanced detection of artifacts in EEG data using higher-order statistics and independent component analysis, Neuroimage. 34 (2007) 1443–1449.

[9] A. Aarabi, K. Kazemi, R. Grebe, H.A. Moghaddam, F. Wallois, Detection of EEG transients in neonates and older children using a system based on dynamic time-warping template matching and spatial dipole clustering, Neuroimage. 48 (2009) 50–62.

[10] A. Klein, W. Skrandies, A reliable statistical method to detect eyeblink-artefacts from electroencephalogram data only, Brain Topogr. 26 (2013) 558–568.

[11] S. Benedetto, M. Pedrotti, L. Minin, T. Baccino, A. Re, R. Montanari, Driver workload and eye blink duration, Transp. Res. Part F. 14 (2011) 199–208.

[12] A. Delorme, S. Makeig, T. Sejnowski, Automatic artifact rejection for EEG data using high-order statistics and independent component analysis, in: Int. Work. ICA, 2001: pp. 457–462.

[13] P. Durka, H. Klekowicz, K. Blinowska, W. Szelenberger, S. Niemcewicz, A simple system for detection of EEG artifacts in polysomnographic recordings, IEEE Trans. Biomed. Eng. 50 (2003) 526–528.

[14] B. Chambayil, R. Singla, R. Jha, EEG eye blink classification using neural network, in: Proc. World Congr. Eng., London, UK, 2010.

[15] S. Vorobyov, A. Cichocki, Blind noise reduction for multisensory signals using ICA and subspace filtering, with application to EEG analysis, Biol. Cybern. 86 (2002) 293–303.

[16] S.-Y. Shao, K.-Q. Shen, C.J. Ong, E.P. V Wilder-Smith, X.-P. Li, Automatic EEG artifact removal: a weighted support vector machine approach with error correction., IEEE Trans. Biomed. Eng. 56 (2009) 336–344.

[17] P. Mishra, S.K. Singla, Artifact removal from biosignal using fixed point ICA algorithm for pre-processing in biometric recognition, Meas. Sci. Rev. 13 (2013) 7–11.

[18] A. Hyvärinen, E. Oja, Independent component analysis: algorithms and applications, Neural Networks. 13 (2000) 411–430.

[19] C.-T. Lin, L.-D. Liao, Y.-H. Liu, I.-J. Wang, B.-S. Lin, J.-Y. Chang, Novel dry polymer foam electrodes for long-term EEG measurement, IEEE Trans. Biomed. Eng. 58 (2011) 1200–1207.

[20] Y. Yasui, A brainwave signal measurement and data processing technique for daily life applications, J. Physiol. Anthropol. 28 (2009) 145–150.

[21] Y. Liu, O. Sourina, M.K. Nguyen, Real-time EEG-based emotion recognition and its applications, Trans. Comput. Sci. XII. 6670 (2011) 256–277.

[22] H.U. Amin, A.S. Malik, N. Badruddin, Brain activation during cognitive tasks: An overview of EEG and fMRI studies, in: IEEE EMBS, 2012: pp. 950–953.

[23] L.-D. Liao, C.-Y. Chen, I.-J. Wang, S.-F. Chen, S.-Y. Li, B.-W. Chen, et al., Gaming control using a wearable and wireless EEG-based brain-computer interface device with novel dry foam-based sensors, J. Neuroeng. Rehabil. 9 (2012) 1–11.

[24] K. Schaaff, T. Schultz, Towards an EEG-based emotion recognizer for humanoid robots, in: IEEE Symp. Robot Hum. Interact. Commun., 2009: pp. 792–796.

[25] J.-S. Lin, W.-J. Yang, S.-H. Liu, Y.-Y. Chang, Implementation of a wireless sensor headband in EEG signal acquisition, in: Recent Adv. CSIE 2011, LNEE 129, 2012: pp. 629–634.

[26] C. Ryu, M. An, Y. Na, J. Cho, A portable neurofeedback system and EEG-analysis methods for evaluation, in: World Congr. Med. Phys. Biomed. Eng. Vol.2, 2007: pp. 1167–1169.

[27] C.-T. Lin, L.-W. Ko, C.-J. Chang, Y.-T. Wang, C.-H. Chung, F.-S. Yang, et al., Wearable and wireless brain-computer interface and its applications, in: Augment. Cogn. HCII 2009, LNAI 5638, 2009: pp. 741–748.

[28] Y.-T. Wang, Y. Wang, T.-P. Jung, A cell-phone-based brain-computer interface for communication in daily life, in: AICI 2010, Part II, LNAI 6320, 2011: pp. 233–240. doi:10.1088/1741-2560/8/2/025018.

[29] J.E. Huggins, P. a. Wren, K.L. Gruis, What would brain-computer interface users want? Opinions and priorities of potential users with amyotrophic lateral sclerosis, Amyotroph. Lateral Scler. 12 (2011) 318–324.

[30] J.E. Huggins, A. a. Moinuddin, A.E. Chiodo, P. a. Wren, What would brain-computer interface users want: opinions and priorities of potential users with spinal cord injury, Arch. Phys. Med. Rehabil. 96 (2015) S38–45.e1–5.

[31] R. Schleicher, N. Galley, S. Briest, L. Galley, Blinks and saccades as indicators of fatigue in sleepiness warnings: looking tired?, Ergonomics. 51 (2008) 982–1010.

[32] K. Fukuda, J.A. Stern, Cognition, blinks, eye-movements, and pupillary movements during performance of a running memory task, Aviat., Space, Environ. Med. 76 (2005) C75–C85.

[33] A. Bulling, J. a Ward, H. Gellersen, G. Tröster, Eye movement analysis for activity recognition using electrooculography, IEEE Trans. Pattern Anal. Mach. Intell. 33 (2011) 741–753.

[34] S. Noachtar, C. Binnie, J. Ebersole, F. Mauguière, A. Sakamoto, B. Westmoreland, A glossary of terms most commonly used by clinical electroencephalographers and proposal for the report form for the EEG findings, in: G. Deuschl, A. Eisen (Eds.), Recomm. Pract. Clin. Neurophysiol. Guidel. IFCN, International Federation of Clinical Neurophysiology, 1999: pp. 21–39.

[35] H.-A.T. Nguyen, J. Musson, F. Li, W. Wang, G. Zhang, R. Xu, et al., EOG artifact removal using a wavelet neural network, Neurocomput. 97 (2012) 374–389.

[36] A.T. Bahill, J.D. McDonald, Frequency limitations and optimal step size for the two-point central difference derivative algorithm with applications to human eye movement data, IEEE Trans. Biomed. Eng. 30 (1983) 191–194. doi:10.1109/TBME.1983.325108.

[37] H. Ghandeharion, A. Erfanian, A fully automatic ocular artifact suppression from EEG data using higher order statistics: Improved performance by wavelet analysis, Med. Eng. Phys. 32 (2010) 720–729.

[38] D.-W. Kim, M. Shim, J.-I. Kim, C.-H. Im, S.-H. Lee, Source activation of P300 correlates with negative symptom severity in patients with schizophrenia, Brain Topogr. (2013) 1–11. doi:10.1007/s10548-013-0306-x.

[39] H. V. Semlitsch, P. Anderer, P. Schuster, O. Presslich, A solution for reliable and valid reduction of ocular artifacts, applied to the P300 ERP, Psychophysiology. 23 (1986) 695–703.

[40] G. Gratton, M.G. Coles, E. Donchin, A new method for off-line removal of ocular artifact., Electroencephalogr. Clin. Neurophysiol. 55 (1983) 468–484.

[41] P.-L. Lee, J.-C. Hsieh, C.-H. Wu, K.-K. Shyu, Y.-T. Wu, Brain computer interface using flash onset and offset visual evoked potentials, Clin. Neurophysiol. 119 (2008) 605–616.

[42] J. Lee, D. Birtles, J. Wattam-Bell, J. Atkinson, O. Braddick, Latency measures of pattern-reversal VEP in adults and infants: different information from transient P1 response and steady-state phase, Invest. Ophthalmol. Vis. Sci. 53 (2012) 1306–1314.

[43] W.-D. Chang, C.-H. Im, Enhanced template matching using dynamic positional warping for identification of specific patterns in electroencephalogram, J. Appl. Math. (2014). doi:10.1155/2014/528071.

[44] S. Kim, J. McNames, Automatic spike detection based on adaptive template matching for extracellular neural recordings, J. Neurosci. Methods. 165 (2007) 165–174.

[45] E.S. Kappenman, S.J. Luck, The effects of electrode impedance on data quality and statistical significance in ERP recordings, Psychophysiol. 47 (2010) 888–904.

[46] R.J. Croft, R.J. Barry, Removal of ocular artifact from the EEG: a review, Clin. Neurophysiol. 30 (2000) 5–19.

[47] R. Verleger, Valid identification of blink artefacts: are they larger than 50 microV in EEG records?, Electroencephalogr. Clin. Neurophysiol. 87 (1993) 354–363.

[48] S. Wang, J. Hu, Design of alignment-free cancelable fingerprint templates via curtailed circular convolution, Pattern Recognit. 47 (2014) 1321–1329.

[49] M.E. Davies, C.J. James, Source separation using single channel ICA, Signal Process. 87 (2007) 1819–1832. doi:10.1016/j.sigpro.2007.01.011.

[50] B. Mijović, M. De Vos, I. Gligorijević, J. Taelman, S. Van Huffel, Source separation from single-channel recordings by combining empirical-mode decomposition and independent component analysis, IEEE Trans. Biomed. Eng. 57 (2010) 2188–2196. doi:10.1109/TBME.2010.2051440.

[51] S. Abbaspour, M. Linden, H. Gholamhosseini, ECG artifact removal from surface EMG signal using an automated method based on wavelet-ICA, Stud. Heal. Technol. Inform. 211 (2015) 1–6.